SUPPLEMENTARY INFORMATION

Trifunctional electrocatalysts based on bimetallic nanoalloy and nitrogen-doped carbon with brush-like heterostructure

Yuyun Irmawati,[‡a,b] Davin Adinata Tan,[‡c] Falihah Balqis,[c] Ferry Iskandar,[d,e,f] and Afriyanti Sumboja[*c,f]

[a]Doctoral Program of Nanosciences and Nanotechnology, Graduate School, Institut Teknologi Bandung, Jl. Ganesha 10, Bandung 40132, Indonesia

[b]Research Center for Advanced Materials, National Research and Innovation Agency (BRIN), Kawasan Puspiptek gedung 440, Tangerang Selatan 15314, Indonesia

[c]Material Science and Engineering Research Group, Faculty of Mechanical and Aerospace Engineering, Institut Teknologi Bandung, Jl. Ganesha 10, Bandung 40132, Indonesia

[d]Department of Physics, Faculty of Mathematics and Natural Science, Institut Teknologi Bandung, Jl. Ganesha 10, Bandung 40132, Indonesia

[e]Research Center for Nanosciences and Nanotechnology, Institut Teknologi Bandung, Jl. Ganesha 10, Bandung 40132, Indonesia

[f]Collaboration Research Center for Advanced Energy Materials, National Research and Innovation Agency - Institut Teknologi Bandung, Jl. Ganesha 10, Bandung 40132, Indonesia.

[*]Email: sumboja@itb.ac.id

[‡]These authors contributed equally to this work.

S1. Experimental Section

Electrochemical measurements: ORR, OER, and HER performance were measured using a rotating disc electrode (RDE) connected to a potentiostat (Autolab PGSTAT302N). The system consisted of a standard three-electrode configuration with Pt sheet counter electrode, Ag/AgCl (3 M KCl solution) reference electrode, and glassy carbon working electrode. Catalyst inks were prepared by dispersing 9 mg of catalysts and 2.25 mg Vulcan XC-72 into a mixed solution of 2087 µL deionized water, 835 µL 2-propanol, and 79 µL Nafion (5 wt%). The prepared catalysts were then drop-casted onto the surface of the glassy carbon until ~0.4 mg cm^{-2} of catalyst loading was acquired. All ORR, OER, and HER performances were measured using linear sweep voltammetry (LSV) with a scan rate of 5 mV sec^{-1} at 1600 rpm. ORR analysis was conducted in 0.1 M KOH, while OER and HER analysis were tested in N_2-saturated of 1 M KOH. All observed potentials were presented relative to the reversible hydrogen electrode (RHE). Furthermore, the ORR stability test was measured via a chronoamperometry test at a constant potential of 0.44 V (vs. RHE). Meanwhile, the OER and HER stability tests were measured via a chronopotentiometry test with a constant current of 2.5 mA cm^{-2} and 10 mA cm^{-2}, respectively.

To calculate the electron transfer number (n), ORR LSV curves were tested at different rotational speeds from 400 to 2500 rpm. The electron transfer number was then calculated by Koutecký-Levich equation ($\frac{1}{j} = \frac{1}{j_k} + \frac{1}{j_l} = \frac{1}{j_k} + \frac{1}{0.62nFAD_{O2}^{\frac{2}{3}}\omega^{\frac{1}{2}}v^{-\frac{1}{6}}C_{o2}^{*}}$), in which F is the Faraday constant, A is the geometric area of glassy carbon, C_{O2} is concentration of O_2 in electrolyte, D_{O2} is oxygen diffusion coefficient, and v is kinematic viscosity of the electrolyte. In 0.1 M KOH, the value of C_{O2} was set at 1.1×10^{-3} mol L^{-1},[1] while D_{O2} and v were 1.86 x 10^{-5} cm^2 s^{-1} and 0.01008 cm^2 s^{-1}, respectively.[2]

Zn-air battery test. Catalyst ink for the Zn-air battery was made by dispersing 4 mg of catalyst and 1 mg of Vulcan XC-72 into 1.8 mL ethanol and 26 µL Nafion (5 wt%). The catalyst ink was then drop-casted into 2x2 cm^2 Teflon-treated carbon paper, resulting in the catalyst loading of about 1 mg cm^{-2}. A mixed catalyst of Pt/C+Ir/C (1:1 w/w) with a similar mass loading was used as the benchmark. The obtained catalyst-loaded carbon paper was then employed as the air-cathode in a Zn-air battery with 6 M KOH + 0.15 M ZnO electrolyte and Zn plate as the anode. The battery's performance was measured via a galvanodynamic discharge-charge test using a potentiostat

(Autolab PGSTAT302N), in which the power density was determined from the discharging curve. Stability tests with charging-discharging cycling tests were conducted at a constant current of 10 mA cm^{-2} using a battery tester (Neware Technology).

Self-powered water electrolyzer. A similar composition of catalyst ink for preparing the air-cathode of Zn-air battery was drop-cated onto 2x1 cm^2 Teflon-treated carbon paper, resulting in the catalyst loading of about 1 mg cm^{-2}. Two identical electrodes with FeCoNC-NB catalyst were prepared as the anode and cathode of water electrolizer in 1 M KOH. Two Zn-air batteries with FeCoNC-NB in a series configuration were then connected to drive the water splitting process.

S2. Supplementary Figures

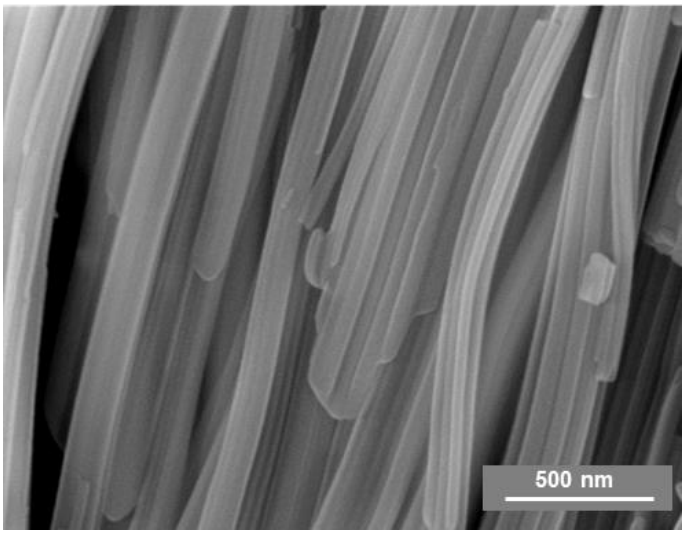

Fig. S1 SEM image of FeCo-NTA wire.

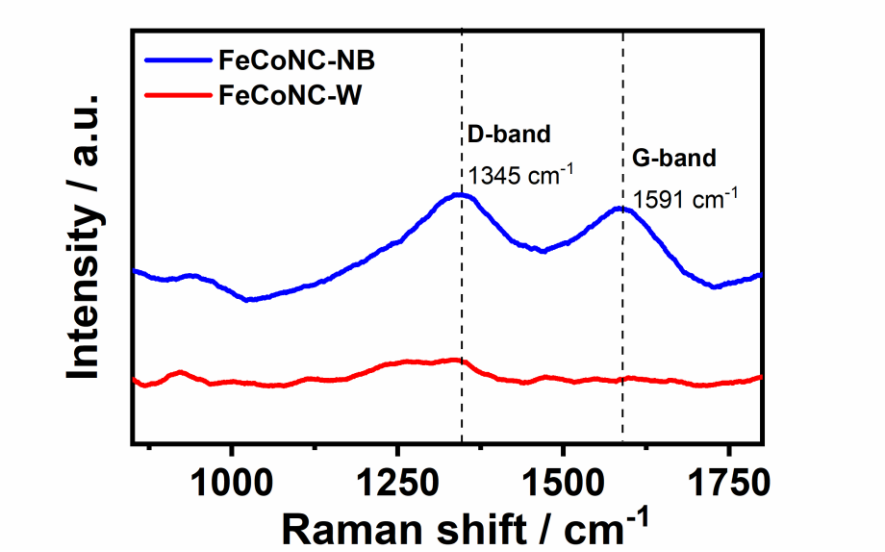

Fig. S2 Raman spectra of FeCoNC-W and FeCoNC-NB.

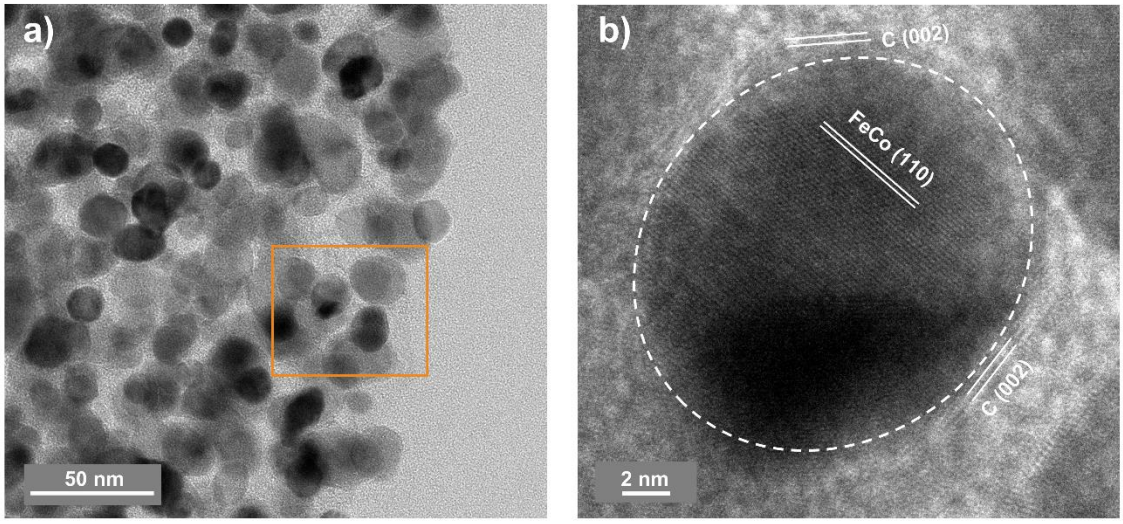

Fig. S3 (a) TEM and (b) HRTEM images of FeCoNC-W.

HRTEM of FeCoNC-W shows lattice fringes with a d-spacing of 0.201 nm that represents the (110) plane of FeCo. Lattice fringes of about 0.34 nm, corresponding to the (002) carbon plane, wraps around the FeCo nanoparticles and constructs FeCo@NC structure.

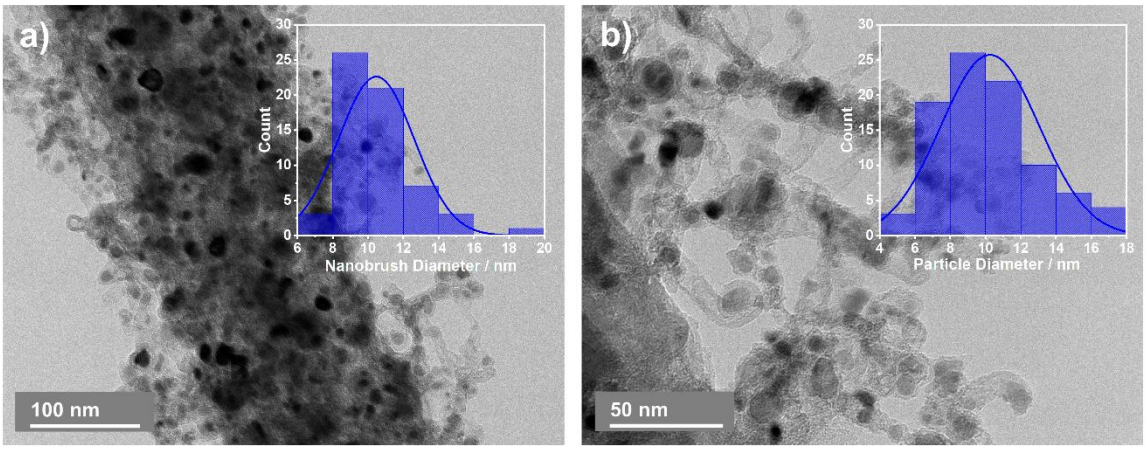

Fig. S4 Size distribution of (a) nanobrushes and (b) nanoparticles on the brush-like structure of FeCoNC-NB sample.

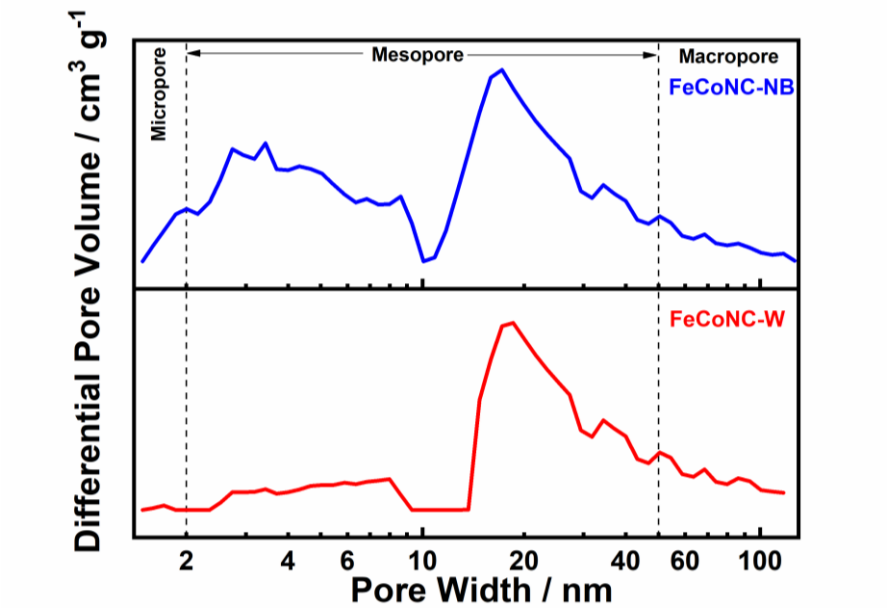

Fig. S5 Pore size distribution of FeCoNC-W and FeCoNC-NB.

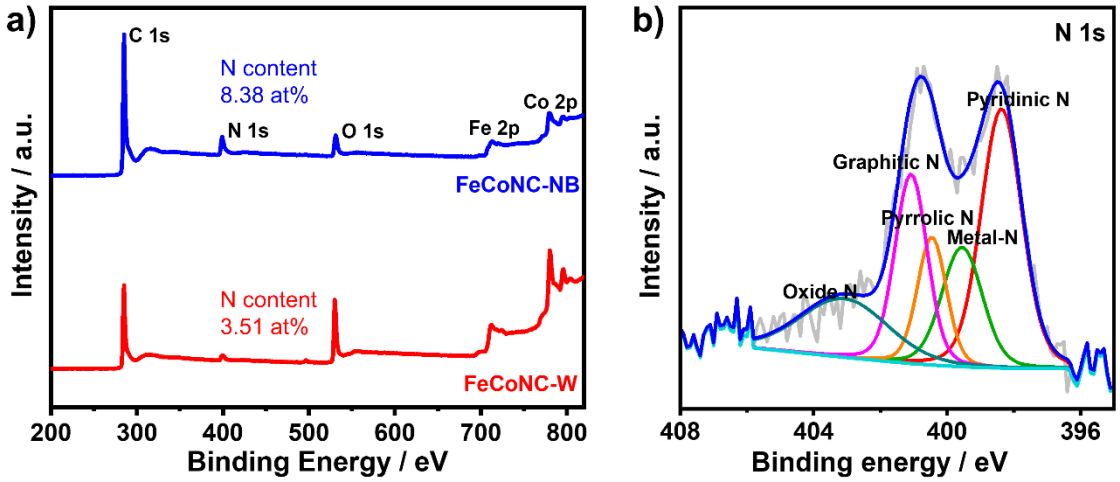

Fig. S6 (a) XPS wide spectra of FeCoNC-W and FeCoNC-NB. (b) N 1s high-resolution XPS spectra of FeCoNC-W.

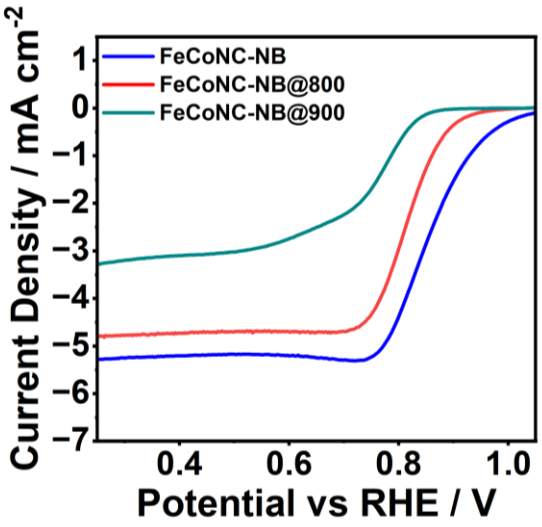

Fig. S7 ORR polarization curves in 0.1 M KOH of the samples prepared at different pyrolysis temperatures: FeCoNC-NB (700 °C), FeCoNC-NB@800 (800 °C), and FeCoNC-NB@900 (900 °C).

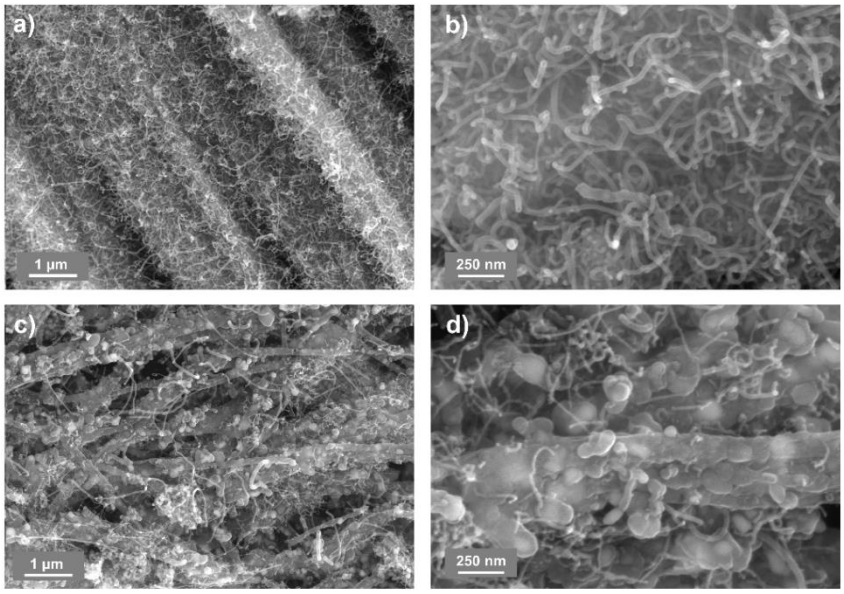

Fig. S8 SEM images of the samples similar to the FeCoNC-NB but prepared at different pyrolysis temperatures: (a-b) 800 °C (FeCoNC-NB@800) and (c-d) 900 °C (FeCoNC-NB@900).

SEM images of FeCoNC-NB@800 show dense and larger carbon nanofibers. This structure may reduce the exposed active sites, thereby reducing the catalytic activity. Meanwhile, a higher pyrolysis temperature of 900 °C (FeCoNC-NB@900) results in a less homogeneous brush-like

structure, formation of larger nanoparticles, and collapse in the primary wire structure. This condition significantly reduces the catalytic activity, in line with the lowest ORR activity of FeCoNC-NB@900 (**Fig. S7**).

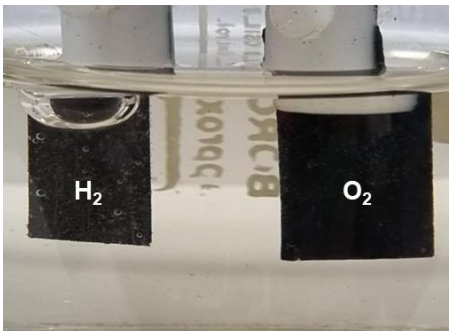

Fig. S9 Digital photos of H_2 and O_2 production in which the self-powered water splitting has been operated for 12 h.

S3. Supplementary Tables

Table S1 Relative content of N species of FeCoNC-W and FeCoNC-NB from XPS measurement.

Species	**Relative content (%) FeCoNC-W**	**Relative content (%) FeCoNC-NB**
Graphitic-N	20.13	14.21
Pyridinic-N	34.80	40.69
Pyrrolic-N	12.19	17.66
Metal-N	15.95	19.27
Oxide-N	16.93	8.17

Table S2 Comparison of ORR activity of FeCoNC-NB in alkaline electrolyte with some reported transition metal-based catalysts.

Catalyst	E_{onset} **(V vs RHE)**	$E_{1/2}$ **(V vs RHE)**	J_L **(mA cm^{-2})**	***n***	**Ref.**
FeCoNC-NB	1.046	0.85	5.38	3.98	This work
FeCo-N/C-hollow spheres	-	0.854	~5.8	3.81	[3]
FeCo-N/C-polyhedral	1.013	0.896	6.35	~4	[4]
FeCo-N/C-hollow cubes	0.91	0.82	5.15	~4	[5]
FeCo/CoP-NP/C-nanofibers	0.85	0.79	~5.4	3.85	[6]
FeCo-N/C-spider web structure	0.89	0.84	~4.8	3.8	[7]
FeCo-N/C-dual sheets/fiber structures	-	0.83	6.45	3.84 - 4	[8]
CoNi-N/C-nanofibers	0.87	0.80	4.9	~4	[9]
FeCoS-N/C-polyhedral	0.94	0.84	~5.4	3.97	[10]
FeCo-N/C-sponges	0.99	0.84	5.93	~4	[11]
FeCoNi-N/C-nanoframes	0.93	0.81	-	~4	[12]
FeCo-N/C-nanosheets	-	0.83	5	3.89	[13]
FeCo-N/C-nanosheets	1.04	0.84	5.23	3.94	[14]

Table S3 Comparison of OER activity of FeCoNC-NB in alkaline electrolyte with some reported transition metal-based catalysts.

Catalyst	**η_{10} (mV vs RHE)**	**Tafel slope (mV dec^{-1})**	**Ref.**
FeCoNC-NB	363	73.1	This work
FeCo-N/C-polyhedral	370	72	[4]
FeCo-N/C-hollow cubes	260	54.6	[5]
FeCo-N/C-dual sheets/fiber structures	290	79	[8]
CoNi-N/C-nanofibers	370	113	[9]
FeCoS-N/C-polyhedral	290	66	[10]
FeCo-N/C-sponges	380	108	[11]
FeCoNi-N/C-nanoframes	270	51	[12]
CoNi-N/C-brush structures	395	74	[15]
CoNi-N/C-nanofibers	315	63.6	[16]

Table S4 Comparison of HER activity of FeCoNC-NB in alkaline electrolyte with some reported transition metal-based catalysts.

Catalyst	η_{10} **(mV vs RHE)**	**Tafel slope (mV dec^{-1})**	**Ref.**
FeCoNC-NB	254	114.2	This work
FeCo/CoP-NP/C-nanofibers	260	120	[6]
Co-N/C-MXene nanosheets	190	78.4	[17]
FeCo-N/C-MoS_2 nanosheets	172	122.4	[18]
Co-N/C-bamboo like fibers	182	105.4	[19]
Co-N/C-leaf like structure	220	128	[20]
CoS-NP/C-polyhedral	183	64.25	[21]
CoNiMn-N/C-hollow polyhedral	191	64.38	[22]
CoMo-N/C-wires	258	126.8	[23]
FeCo-N/C-nanofibers	249	172	[24]
Co-N/C-nanosheets	262	84	[25]

Table S5 Performance comparison of Zn-air batteries with some reported transition metal-based catalysts in alkaline electrolyte. ($\triangle E$ ORR/OER = E_{10} of OER - $E_{1/2}$ of ORR).

Catalyst	**$\triangle E$ ORR/OER (V)**	**P_{max} (mW cm^{-2})**	**Cycle time (hours)**	**Ref.**
FeCoNC-NB	0.743	195	350 at 10 mA cm^{-2}	This work
FeCo/CoP-NP/C-nanofibers	0.77	154	107 at 10 mA cm^{-2}	[6]
FeCo-N/C-spider web structure	0.75	107.6	118 at 10 mA cm^{-2}	[7]
Co-N/C	0.85	80.17	140 at 10 mA cm^{-2}	[26]
FeCo-N/C-cruciform	0.71	145	445 at 10 mA cm^{-2}	[27]
Co-N/C-microsphere	0.76	141.6	51.7 at 5 mA cm^{-2}	[28]
FeNi-N/C	0.75	137.7	100 at 5 mA cm^{-2}	[29]
Co-N/C-nanofibers	0.76	179.3	100 at 5 mA cm^{-2}	[30]
CoCr-N/C-nanosheets	0.73	100.5	100 at 10 mA cm^{-2}	[31]

Table S6 Performance comparison of FeCoNC-NB with some recently reported trifunctional catalysts in alkaline electrolyte. ($\triangle E$ HER/OER = E_{10} of OER – E_{10} of HER).

Catalyst	$E_{1/2}$ **of ORR (V)**	η_{10} **of OER (mV)**	η_{10} **of HER (mV)**	$\triangle E$ **HER/OER (V)**	**Ref.**
FeCoNC-NB	0.85	363	254	1.847	This work
FeCo/CoP-NP/C-nanofibers	0.79	330	260	1.820	[6]
FeCo-N/C-spider web structure	0.84	360	200	1.790	[7]
CoNi-N/C-brush structures	0.80	395	150	1.775	[15]
FeCo-N/C-nanofibers	0.86	388	249	1.867	[24]
Co-N/C-nanosheets	0.82	280	262	1.772	[25]
FeCo-N/C-cruciform	0.84	320	151	1.700	[27]
FeCoNi-N/C	0.88	320	274	1.824	[32]
FeC-Co-N/C	0.88	340	238	1.808	[33]
Co-N/C-brush structures	0.78	390	190	1.810	[34]
CoS-N/C-spheres	0.79	460	330	2.020	[35]
FeCo-N/C	0.85	380	164	1.774	[36]
CoN-N/C	0.86	340	210	1.780	[37]
FeCo-N/C-sponge	0.83	380	233	1.843	[38]

References

1. J. Gao, M. Zhou, X. Wang, H. Wang, Z. Yin, X. Tan and Y. Li, *Batteries*, 2022, **8**, 150.
2. F. W. T. Goh, Z. Liu, X. Ge, Y. Zong, G. Du and T. S. A. Hor, *Electrochim. Acta*, 2013, **114**, 598-604.
3. S. L. Zhang, B. Y. Guan and X. W. Lou, *Small*, 2019, **15**, 1805324.
4. X. Duan, S. Ren, N. Pan, M. Zhang and H. Zheng, *J. Mater. Chem. A*, 2020, **8**, 9355-9363.
5. D. Xie, D. Yu, Y. Hao, S. Han, G. Li, X. Wu, F. Hu, L. Li, H.-Y. Chen, Y.-F. Liao and S. Peng, *Small*, 2021, **17**, 2007239.
6. Q. Shi, Q. Liu, Y. Ma, Z. Fang, Z. Liang, G. Shao, B. Tang, W. Yang, L. Qin and X. Fang, *Adv. Energy Mater.*, 2020, **10**, 1903854.
7. F. Wang, Z. Xiao, X. Liu, J. Ren, T. Xing, Z. Li, X. Li and Y. Chen, *J. Power Sources*, 2022, **521**, 230925.

8. X. Wang, H. Xu, S. Huang, X. Zeng, L. Li, X. Zhao and W. Zhang, *Appl. Surf. Sci.*, 2023, **609**, 155452.
9. Y. Xie, C. Feng, Y. Guo, S. Li, C. Guo, Y. Zhang and J. Wang, *Appl. Surf. Sci.*, 2021, **536**, 147786.
10. T. Liu, F. Yang, G. Cheng and W. Luo, *Small*, 2018, **14**, 1703748.
11. C. Chen, Y. Li, D. Cheng, H. He and K. Zhou, *ACS Appl. Mater. Interfaces*, 2020, **12**, 40415-40425.
12. Q. Wang, L. Shang, R. Shi, X. Zhang, G. I. N. Waterhouse, L.-Z. Wu, C.-H. Tung and T. Zhang, *Nano Energy*, 2017, **40**, 382-389.
13. Q. Xu, H. Jiang, Y. Li, D. Liang, Y. Hu and C. Li, *Appl. Catal. B*, 2019, **256**, 117893.
14. S. Yang, Y. Yu, M. Dou, Z. Zhang, L. Dai and F. Wang, *Angew. Chem., Int. Ed.*, 2019, **58**, 14724-14730.
15. J. Li, J. Qian, X. Chen, X. Zeng, L. Li, B. Ouyang, E. Kan and W. Zhang, *Compos. B. Eng.*, 2022, **231**, 109573.
16. T. Zhao, Z. Song, X. Wang and J. Gao, *J. Solid State Chem.*, 2023, **326**, 124213.
17. L. Zhang, X. Zhao, Z. Chu, Q. Wang, Y. Cao, J. Li, W. Lei, J. Cao and W. Si, *Int. J. Hydrog. Energy*, 2023, **48**, 15053-15064.
18. W. Ma, W. Li, H. Zhang and Y. Wang, *Int. J. Hydrog. Energy*, 2023, **48**, 22032-22043.
19. Z.-J. Jiang, G. Xie, L. Guo, J. Huang and Z. Jiang, *Electrochim. Acta*, 2020, **342**, 136076.
20. S. Gayathri, P. Arunkumar, R. Bose, A. Alfantazi and J. H. Han, *Chem. Eng. J.*, 2021, **426**, 131270.
21. L. Zhao, A. Yang, A. Wang, H. Yu, J. Dai and Y. Zheng, *Int. J. Hydrog. Energy*, 2020, **45**, 30367-30374.
22. B. Jiang and Z. Li, *J. Solid State Chem.*, 2021, **295**, 121912.
23. L. Yang, J. Yu, Z. Wei, G. Li, L. Cao, W. Zhou and S. Chen, *Nano Energy*, 2017, **41**, 772-779.
24. W. Yang, J. Guo, J. Ma, N. Wu, J. Xiao and M. Wu, *J. Alloys Compd.*, 2022, **926**, 166937.
25. J. Liu, C. Wang, H. Sun, H. Wang, F. Rong, L. He, Y. Lou, S. Zhang, Z. Zhang and M. Du, *Appl. Catal. B*, 2020, **279**, 119407.
26. X. Zhang, J. Xu and L. Wu, *Mater. Today Sustain.*, 2022, **19**, 100180.
27. G. Zhou, G. Liu, X. Liu, Q. Yu, H. Mao, Z. Xiao and L. Wang, *Adv. Funct. Mater.*, 2022, **32**, 2107608.
28. M. Tan, Y. Xiao, W. Xi, X. Lin, B. Gao, Y. Chen, Y. Zheng and B. Lin, *J. Power Sources*, 2021, **490**, 229570.
29. J. Chen, L. Li, Y. Cheng, Y. Huang and C. Chen, *Int. J. Hydrog. Energy*, 2022, **47**, 16025-16035.
30. B. Gao, M. Tan, W. Xi, X. Lin, Z. Li, M. Shen and B. Lin, *J. Power Sources*, 2022, **527**, 231205.
31. S. Zhao, S. Ran, N. Shi, M. Liu, Y. Zeng, W. Sun and Z. Zhu, *Int. J. Hydrog. Energy*, 2022, **47**, 30449-30459.
32. R. Jiang, D. R. Baker, D. T. Tran, J. Li, A. C. Leff and S. S. Zhang, *ACS Appl. Nano Mater.*, 2020, **3**, 7119-7129.
33. C. C. Yang, S. F. Zai, Y. T. Zhou, L. Du and Q. Jiang, *Adv. Funct. Mater.*, 2019, **29**, 1901949.
34. X. Yao, J. Li, Y. Zhu, L. Li and W. Zhang, *Compos. B. Eng.*, 2020, **193**, 108058.

35. Q. Ju, R. Ma, Y. Pei, B. Guo, Q. Liu, T. Zhang, M. Yang and J. Wang, *Mater. Res. Bull.*, 2020, **125**, 110770.
36. S. M. Alshehri, A. N. Alhabarah, J. Ahmed, M. Naushad and T. Ahamad, *J. Colloid Interface Sci.*, 2018, **514**, 1-9.
37. X. Lv, Z. Xiao, H. Wang, X. Wang, L. Shan, F. Wang, C. Wei, X. Tang and Y. Chen, *J. Energy Chem.*, 2021, **54**, 626-638.
38. H. Liu, D.-H. Yang, X.-Y. Wang, J. Zhang and B.-H. Han, *J. Colloid Interface Sci.*, 2021, **581**, 362-373.